Chinese Chemical Letters 33 (2022) 1632–1636

Contents lists available at ScienceDirect

Chinese Chemical Letters

journal homepage: www.elsevier.com/locate/cclet

Carbon dot-based fluorescent and colorimetric sensor for sensitive and selective visual detection of benzoyl peroxide

Xiangcao Li[a,1], Xuejian Xing[a,1], Shaojing Zhao[a], Shaohua Zhu[c], Benhua Wang[a], Minhuan Lan[a,b,*], Xiangzhi Song[a]

[a] Key Laboratory of Hunan Province for Water Environment and Agriculture Product Safety, College of Chemistry and Chemical Engineering, Central South University, Changsha 410083, China
[b] Shenzhen Research Institute of Central South University, Shenzhen 518057, China
[c] Hunan Norui Environmental Technology Co., Ltd., Changsha 410021, China

ARTICLE INFO

Article history:
Received 19 May 2021
Revised 23 September 2021
Accepted 23 September 2021
Available online 30 September 2021

Keywords:
Carbon dots
Benzoyl peroxide
Colorimetric
Fluorescent probe
Food safety

ABSTRACT

Benzoyl peroxide (BPO) has been added in wheat flour because of its bleaching effect. However, the abnormal used BPO has caused increasing concern due to its strong oxidization capability which may have adverse effects on living organisms. Herein, we present a carbon dot (CD)-based fluorescent and colorimetric probe for visually, sensitively and selectively sensing BPO. The addition of BPO could quench the red fluorescence of CDs peaked at 622 and 677 nm, and decrease the absorbance at 613 nm, while increase the absorbance at 450 nm, resulting in a fluorescence turn-off and colorimetric spectral response. Moreover, the CDs had short response time of 10 min and high sensitivity towards BPO with a low limit of detection of 28 nmol/L. The applicability of the CDs in detecting BPO in wheat, noodle and starch samples was further demonstrated, and good recovery results were obtained.

Benzoyl peroxide (BPO) has been widely used as a brightener in wheat flour in many countries due to its bleaching and sanitizing abilities [1,2]. However, recent studies revealed that BPO not only destroys the nutrients in wheat flour, but also causes many adverse effects to human health because the strong oxidization capacity [3]. Moreover, benzoic acid, biphenyl and phenyl benzoate which may damage health tissue were generated when BPO was decomposed [4]. In 2011, the Chinese government has prohibited BPO used in wheat flour-derived food [5]. However, it should be noted that BPO is still being illegally added to food samples [6].

Although gas chromatography [7], mass spectrometry [8], high-performance liquid chromatography [9], chemiluminescence [10], and electrochemistry [11] methods have been developed to probe BPO in wheat flour-derived foods, these techniques need complicate instruments and time-cost pretreatment processes, which have restricted their practical applications. Optical sensors, such as colorimetric and fluorescent sensors, have been increasingly used for detecting trace amounts of heavy metal ions [12], biomolecules [13], and chemical pollutants [14], because of their simple operation and fast spectroscopic response. For instance, Tian *et al.* prepared a hemicyanine dye which can detect BPO in food samples based on a fluorescent "off-on" approach [15]. Li *et al.* synthesized a coumarin derivative that exhibits colorimetric and fluorometric spectral response to BPO [16]. Recently, Zhu *et al.* designed a novel biomass curcumin-based ionic liquid (CIL) that exhibits colorimetric and fluorescent signals in BPO detection [17]. However, these probes suffer from complex synthesis and purification processes, as well as poor water solubility and photostability [18]. Moreover, most of these probes cannot differentiate BPO from H_2O_2. Recently, Li *et al.* fabricated 4-mercaptophenylboronic acid (MPBA)-modified AuNPs and dopamine-modified AuNPs-nanoassembled probe for colorimetric detection of BPO, which was achieved by deboronation mechanism [19]. However, many other factors may also induce the aggregation of AuNPs, and it is still having great challenge to design excellent optical probes to rapidly, sensitively, and selectively detect BPO.

Fluorescent carbon dots (CDs) have attracted great attention due to their excellent biocompatibility, tunable photochemical and photophysical properties, good photostability, easy synthesis and surface modification methods [20]. Therefore, kinds of CDs have been used in fluorescent sensing and imaging [21]. Herein, we prepared red fluorescent CDs which can sensitively

* Corresponding author at: Key Laboratory of Hunan Province for Water Environment and Agriculture Product Safety, College of Chemistry and Chemical Engineering, Central South University, Changsha 410083, China.
E-mail address: minhuanlan@csu.edu.cn (M. Lan).
[1] These authors contributed equally to this work.

https://doi.org/10.1016/j.cclet.2021.09.086
1001-8417/

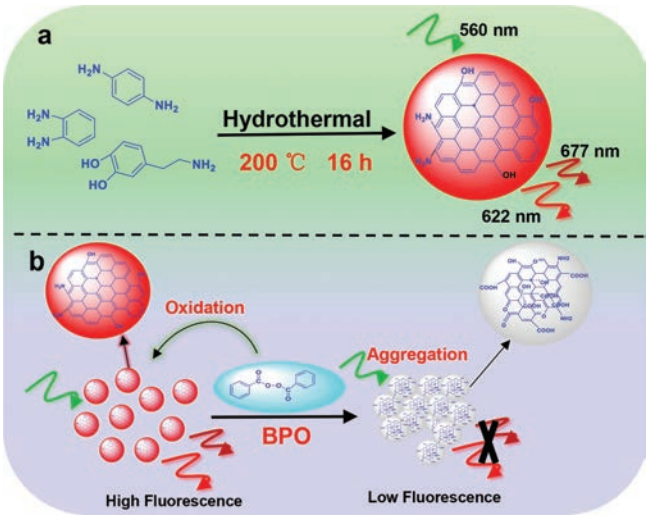

Scheme 1. Schematic illustration (a) the synthesis of CDs and (b) fluorescence quenching mechanism of CDs during BPO sensing.

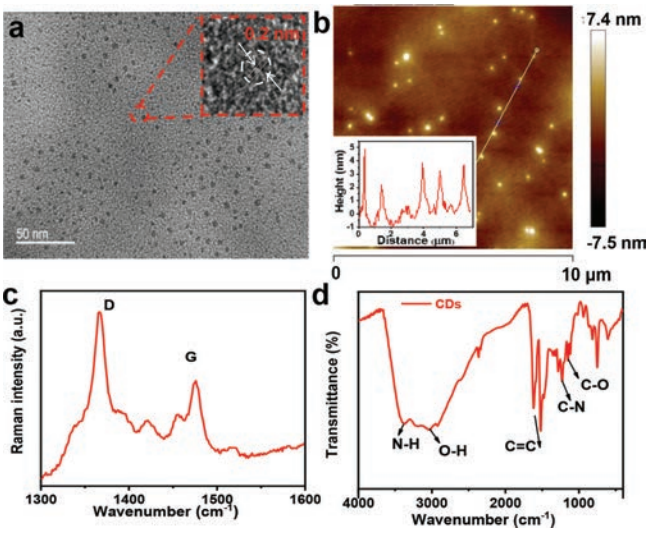

Fig. 1. Characterization of CDs. (a) TEM and HR-TEM images, (b) AFM image and section analysis (inset: the height of CDs in AFM), (c) Raman spectrum, and (d) FTIR spectrum of CDs. Scale bar: 50 nm.

and selectively detect BPO with colorimetric and fluorescent "turn-off" spectral response. As revealed in Scheme 1, the CDs were prepared by hydrothermal treatment of *p*-phenylenediamine, *o*-phenylenediamine, and dopamine under 200 °C for 16 h. The obtained CDs emit strong red fluorescence peaks at 622 and 677 under 560 nm excitation. The addition of BPO can oxidize the C=C bonds into -OH or -COOH groups, neutralize the positively charged $-NH_2$ groups on the surface of CDs, and form multiple hydrogen bonds among CDs, which result in producing large particles and quenching the fluorescence. The solution color of CDs was changed from blue to yellow. This probe also had short response time, as well as high sensitivity and selectivity towards BPO in buffer solution and in wheat flour, noodle, and starch samples. In addition, the red fluorescence CDs can avoid the interference of some blue fluorescent proteins in food samples, which provides practical application opportunities.

CDs were synthesized by hydrothermal method using *p*-phenylenediamine, *o*-phenylenediamine, and dopamine as the sources and HCl aqueous solution as the solvent. Fig. 1a shows the TEM image of the obtained CDs, revealing the uniform size

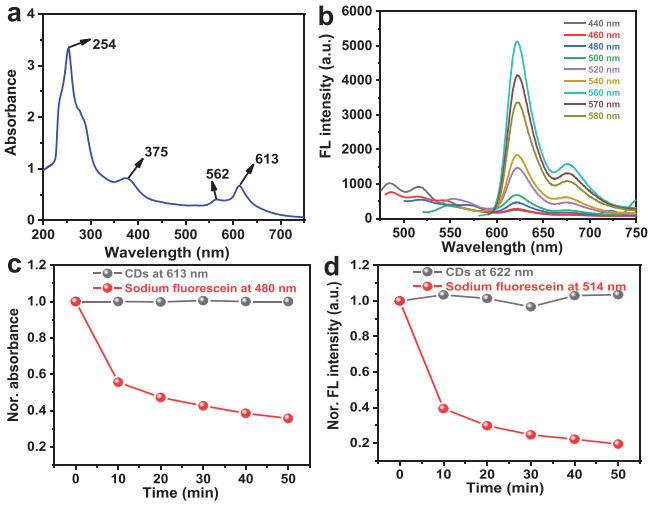

Fig. 2. Optical properties of CDs. (a) UV-vis absorption spectrum of CDs. (b) Fluorescence spectra of CDs obtained under different excitation wavelengths from 440 nm to 580 nm. Time-dependent normalized (c) absorbance and (d) fluorescence intensity of CDs and sodium fluorescein under xenon lamp (1 W/cm^2) irradiation for 50 min. The excitation wavelengths of CDs and sodium fluorescein are 560 nm and 440 nm, respectively.

and morphology with an average diameter of 3.65 nm (Fig. S1 in Supporting information). Clearly crystalline structure with interlayer lattice fringes of 0.20 nm was observed in the high-resolution TEM image of one CD (Fig. 1a, inset). The height of CDs was measured to be ~3.3 nm from the AFM image (Fig. 1b), which is agree well with the TEM observation. The Raman spectrum of CDs exhibited two graphene-like bands, *i.e.*, the G band peaked at 1476 cm^{-1} and D band peaked at 1367 cm^{-1}, with the intensity ratio (I_G/I_D) of 0.79, indicating that the lattice defect and disordered carbon are the main composition (Fig. 1c) [22,23]. The FT-IR spectrum showed a broad vibrational absorption band of O-H/N-H at 3100–3400 cm^{-1}. Two sharp stretching vibration bands of C=C peaked at 1617 and 1523 cm^{-1} were observed. The two peaks at 1280 and 1230 cm^{-1} were correspondent to the C-N bond, and a peak at 1147 cm^{-1} was ascribed to the C-O stretching vibration (Fig. 1d) [24]. Moreover, the XRD pattern of the CDs showed an obvious diffraction peak at $2\theta = 25°$, which can be attributed to the graphite carbon [002] plane (Fig. S2 in Supporting information). Besides, the zeta potential of CDs was measured to be +28.4 mV, suggesting the presence of abundant $-NH_2$ groups on the surface.

To investigate the elemental and surface chemical compositions of the CDs more clearly, X-ray photoelectron spectroscopy (XPS) was conducted. The survey spectrum of the CDs shown in Fig. S3a (Supporting information) exhibited four peaks at 198.0, 284.9, 399.7, and 533.1 eV, which are originated from the Cl 2p, C 1s, N 1s, and O 1s, respectively. The ratio of C/N/O/Cl was calculated to be 74.7/13.6/6.2/5.5. The high resolution XPS spectrum for C 1s shown in Fig. S3b (Supporting information) was divided into three peaks, *i.e.*, 284.4, 284.7, and 290.6 eV, corresponding to C-C, C-O/C-N, and C=O, respectively. The N 1s spectrum in Fig. S3c (Supporting information) was divided into three peaks, including 398.8, 399.7, and 400.8 eV, attributing to the pyridinic N, pyrrolic N, and amino N. Additionally, the peaks of C=O, C-O, and O-H were also observed in the O 1s spectrum in Fig. S3d (Supporting information) [25]. These analyses are consistent with the FT-IR results, suggesting number of -OH, -COOH and $-NH_2$ groups are presented on the surface of CDs.

To investigate the optical properties of CDs, the UV-vis absorption spectrum of the obtained CDs exhibited a broad absorption from 200 nm to 720 nm (Fig. 2a). The absorption peaked at 254

and 375 nm are originated from the π-π^* transition of C=C, while the absorption peaked at 562 and 613 nm are due to the n-π^* transition of C=O, demonstrating that there is the large-sized conjugated sp^2 domain [26,27]. The fluorescence spectra of CDs under different excitation wavelengths were presented in Fig. 2b, two emission peaks at 622 and 677 nm caused by the large-sized conjugated sp^2 domain were observed [28], and the maximum fluorescence intensity was obtained when the excitation wavelength was 560 nm. However, the emission wavelengths show no obvious change when the excitation wavelength increased from 440 nm to 580 nm, suggesting that the CDs have homogeneous nanostructure and surface chemical states. The fluorescence quantum yield of the CDs aqueous solution (pH 7) was calculated as 22.4% with the usage of rhodamine B as the standard.

Then, we conducted the experiments with the comparison with sodium fluorescein to test the photostability and anti-photobleaching ability of CDs. As shown in Fig. 2c and Figs. S4a and b (Supporting information), after 50 min of a xenon lamp irradiation under 1 W/cm^2, the absorbance at 613 nm of CDs was nearly unchanged, while that at 480 nm of sodium fluorescein was decreased significantly. Additionally, the CDs showed better anti-photobleaching ability than sodium fluorescein (Fig. 2d, Figs. S4c and d in Supporting information). These results confirmed that the CDs have eminent photostability and anti-photobleaching ability, which are the two prerequisites required that the advanced optical sensing systems ought to possess.

Considering their favorable precondition, CDs were expected to accurately and reliably detect BPO. The influence of pH on the optical properties of CDs was further studied. As presented in Fig. S5a (Supporting information), the absorbance at 613 nm of CDs was gradually decreased with increasing pH, while the solution color was changed from blue to red (inset of Fig. S5 in Supporting information). The highest fluorescent intensity was observed when CDs were dissolved in aqueous solution at pH 2, while the fluorescent intensity significantly decreased with further increasing pH value (Figs. S5b and c in Supporting information). This may be due to the surface -NH_2 groups were protonated under acidic conditions, allowing them to become monodisperse through electrostatic repulsion, resulting in a strong red fluorescence. Conversely, the CDs were deprotonated under alkaline conditions, causing the aggregation state and forming large particles which induced the quenching of the fluorescence [29]. Thus, subsequent experiments were carried out at pH 2.

The interaction between CDs and BPO at a buffer solution with pH 2 was further studied. As revealed in Fig. 3a, upon the addition of BPO, the absorbance at 613 nm of the CDs was decreased, while that at 450 nm was gradually increased, and a good linear relationship between the A_{613}/A_{450} ratio of the CDs and the concentrations of BPO from 25 μmol/L to 125 μmol/L was observed (Fig. S6 in Supporting information). The color of the CDs aqueous solution was changed from blue to yellow (Fig. 3a, inset). Due to the high fluorescence quantum yield, the concentration of CDs in the fluorescence spectral detection was much lower than that in the absorption spectra. As presented in Fig. 3b, the fluorescence of CDs appeared gradually quenching by BPO (from 0.25 μmol/L to 2.5 μmol/L), as shown in Fig. 3c, and a good linear relationship was observed when the BPO concentrations ranging from 0.25 μmol/L to 1.5 μmol/L, as shown in Fig. S7 (Supporting information). The detection limit was thus calculated to be ~28 nmol/L, demonstrating the CDs could be used as a colorimetric and fluorescent probe for sensitive detection of BPO.

To explore the impact of individual carbon source on the optical properties and detection for BPO, we have prepared other three CDs (named CDs-1, CDs-2, and CDs-3) by using *p*-phenylenediamine, *o*-phenylenediamine, and dopamine as the carbon source, respectively, and HCl aqueous solution as the solvent

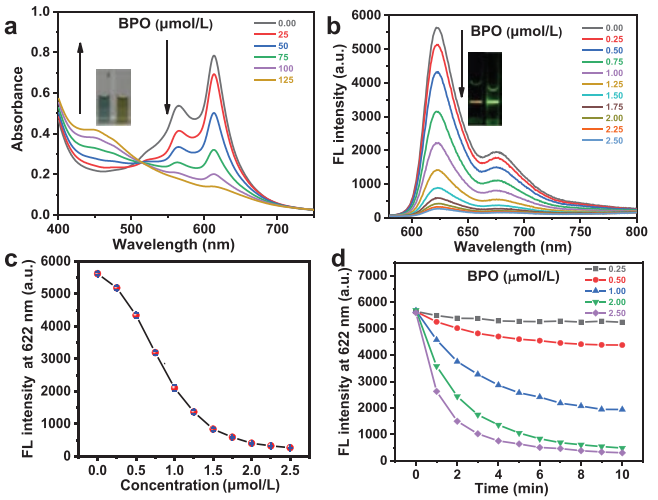

Fig. 3. (a) UV-vis absorption spectra of CDs (60 mg/L) upon gradual addition of BPO from 25 μmol/L to 125 μmol/L. The inset shows the photographs of CDs aqueous solution in the absence (left) and the presence (right) of 125 μmol/L BPO. (b) Fluorescence spectra of CDs (0.7 mg/L) upon gradual addition of BPO from 0.25 μmol/L to 2.5 μmol/L. The inset shows the fluorescence color of CDs aqueous solution in the absence (left) and the presence (right) of 2.5 μmol/L BPO upon being irradiated with green laser. (c) Linear plot of fluorescent intensity at 622 nm of CDs versus BPO concentrations from 0.25 μmol/L to 2.5 μmol/L. (d) Time-dependent fluorescent intensities at 622 nm of CDs upon the addition of 0.25, 0.5, 1.0, 2.0, and 2.5 μmol/L BPO.

under the same reaction condition. As shown in Fig. S8a (Supporting information), the absorption spectrum of CDs-1 showed two absorbance peaked at 373 and 453 nm in pH 2 aqueous solution, upon increasing the pH of the solution, the absorbance at 453 was decreased. The corresponding fluorescence spectra of the CDs-1 were shown in Fig. S8b (Supporting information), two emission peaks at ~628 and 675 nm, and the highest fluorescent intensity were observed in pH 2 buffer solution. Upon addition of BPO, the fluorescence of CDs-1 was quenched, as shown in Fig. S8c (Supporting information). However, the sensitivity toward BPO detection is much lower than the CDs prepared from *p*-phenylenediamine, *o*-phenylenediamine, and dopamine. Similarly, the absorbance at the long wavelength and fluorescent intensity of CDs-2 and CDs-3 were decreased upon increasing the pH of the solution (Fig. S9 in Supporting information). The fluorescence of CDs-2 and CDs-3 are too weak to detection BPO.

The response time is a key parameter for the practical sensing application of sensor. As shown in Fig. 3d, after adding different concentrations of BPO (0.25, 0.5, 1.0, 2.0, and 2.5 μmol/L), the fluorescent intensity of CDs aqueous solution was decreased and then reached a plateau at 10 min, indicating that the reaction time is 10 min, which is faster than most previously reported BPO probes (Table S1 in Supporting information).

In addition to response time, the selectivity of CDs towards BPO is also an important factor in practical sensing application, thus, the selectivity of CDs towards BPO was examined by collecting the fluorescence spectra of CDs in the presence of various species that might co-exist with BPO. As shown in Figs. 4a–c, the addition of metal ions, anion and amino acids showed no obvious effect on the fluorescence of CDs, only the addition of BPO could quench the fluorescence. Moreover, in the presence of these interferences, especially, H_2O_2, the added BPO could still quench the fluorescence of CDs which suggested its excellent selectivity and strong anti-interference performance toward BPO. It may be attributed to the strong oxidizing properties than other substances. In addition, the presence of hydrogen bonds between CDs and the product of BPO decomposition can also cause the aggregation of CDs.

Table 1
The detection of the spiked BPO in wheat, noodle and starch samples by CDs.

Sample	Spiked (μmol/L)	Found (μmol/L)	Recovery (%)[a]	RSD (%, n= 3)
Wheat flour	0.50	0.48 ± 0.01	96.00	0.10
	0.75	0.81 ± ± 0.03	107.00	0.50
	1.00	1.05 ± 0.02	105.00	1.45
Noodle	0.50	0.49 ± 0.01	98.00	0.48
	0.75	0.77 ± 0.02	103.00	1.50
	1.00	1.03 ± 0.03	103.00	2.70
Starch	0.50	0.52 ± 0.02	104.00	1.66
	0.75	0.76 ± 0.04	101.00	3.24
	1.00	1.02 ± 0.02	102.00	1.73

[a] Recovery (%) = [(Found value-blank value)/spiked value] × 100%.

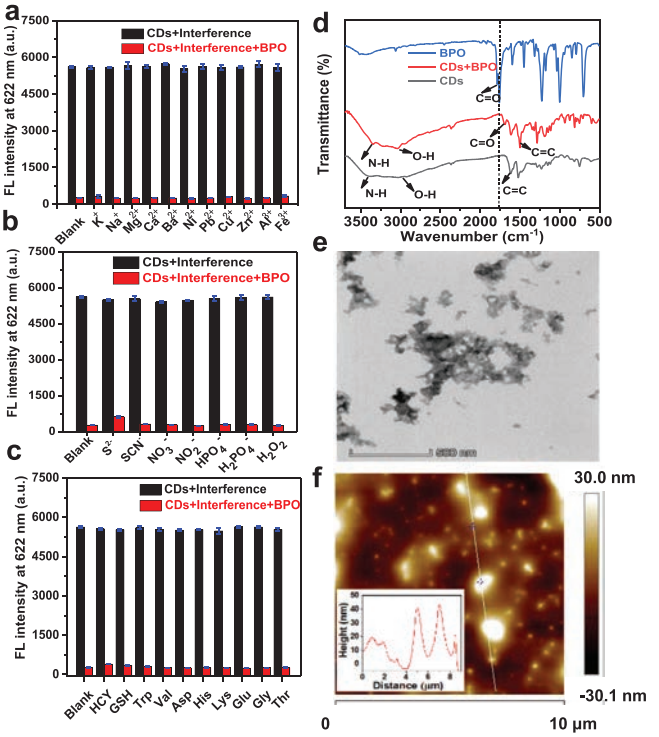

Fig. 4. Fluorescence intensity of CDs (0.7 mg/L) in the presence of interferences (black columns) and interferences + BPO (red columns); reaction time: 10 min. The interferences include: (a) NO_2^-, H_2O_2, MnO_2, $Na_2S_2O_5$, $NaIO_4$, ZnS_2O_8, Na_2SO_3, $NaHSO_3$, $O_2^{\bullet-}$, $^{\bullet}OH$, and $^1O_2$; (b) K^+, Na^+, Mg^{2+}, Ca^{2+}, Ba^{2+}, Ni^{2+}, Pb^{2+}, Cu^{2+}, Zn^{2+}, Al^{3+}, and Fe^{3+}; (c) homocysteine (Hcy), glutathione (GSH), tryptophan (Trp), valine (Val), aspartate (Asp), histidine (His), lysine (Lys), glutamic (Glu), glycine (Gly), and threonine (Thr). (d) FTIR spectra of CDs, BPO, and CDs + BPO. (e) TEM image of CDs in the presence of BPO. (f) AFM image of CDs in the presence of BPO.

According to the above test and analysis about selectivity, we further investigate sensing mechanism, the zeta potential of the CDs in the absence and presence of BPO were measured. The results showed that the zeta potential of the CDs solution was decreased from +28.4 mV to −0.706 mV after adding BPO, suggesting that the C=C bonds in CDs were oxidized into -OH or -COOH groups, which could then not only neutralize the positively charged -NH_2 groups on the surface of CDs, but also form multiple hydrogen bonds with CDs, both of which can lead to producing large particles and effectively quench the fluorescence of CDs. Moreover, the FT-IR spectra in Fig. 4d revealed that the vibrational absorption of C=C at 1618 cm^{-1} was weakened, and that of the C=O at 1690 cm^{-1} appeared upon addition of BPO, this also suggests that the C=C bonds were oxidized into -COOH groups. Furthermore, the BPO induced aggregates were clearly observed in the TEM and AFM images (Figs. 4e and f). Besides, the Tyndall effect occurred in the solution irradiated with red laser (Fig. S10 in Supporting information). The above observations indicate that large particles were formed.

Due to its brightening effect, BPO is often employed as a food additive in wheat flour, noodle, and starch, however, excessive use of BPO can cause damages to human health. From a practical point of view, the ability of the probe to monitor BPO accurately in real food samples is a very crucial factor determining its performance. Consequently, we performed an experiment to determine the spiked BPO in wheat flour, noodle and starch through the standard addition method, and the food samples were purchased from supermarket in Changsha, China. BPO in these real food samples were first extracted with EtOH and then the supernatant was centrifuged for 10 min and filtered with 0.22 μm membrane. After the addition of extracts without spiked BPO, the fluorescence intensity of CDs at 622 nm was obviously decreased, suggesting a certain amount of BPO existed in these food samples. Then the food sample solution was spiked with 0.50, 0.75, 1.00 μmol/L amounts of BPO (Table 1). The recovery was found to be good, demonstrating that the CDs could be reliably used as a probe for detecting BPO in real food samples.

Herein we prepared a red fluorescent CDs with high quantum yield of 22.4% through controlled thermal pyrolysis of *p*-phenylenediamine, *o*-phenylenediamine, and dopamine. The obtained CDs could be used as colorimetric and fluorescent probe for the sensitivity, selectivity and quick detection of BPO in a reliable manner. The sensing mechanism was proposed that the strong oxidizability of BPO could break the conjugate system and produce many -COOH and -OH groups which can form multiple hydrogen bonds among CDs and neutralize their surface charge, significantly inducing the aggregation of CDs. Finally, the detection of BPO in wheat, noodle and starch samples was demonstrated, and satisfactory recovery result was observed.

Declaration of competing interest

The authors declare that they have no known competing financial interests or personal relationships that could have appeared to influence the work reported in this paper.

Acknowledgments

This work was supported by National Natural Science Foundation of China (Nos. 61805287, 62175262), Natural Science Foundation of Hunan Province, China (No. 2019JJ50824), Fundamental Research Funds for the Central South Universities (Nos. 2020CX021, 2020zzts387), and Basic Research Foundation of Shenzhen Science and Technology Innovation (No. JCYJ20180307151245919).

Supplementary materials

Supplementary material associated with this article can be found, in the online version, at doi:10.1016/j.cclet.2021.09.086.

References

[1] L.T. Zeng, X.L. Wu, Q. Hu, H.Q. Yuan, G.M. Bao, Sens. Actuators B: Chem. 299 (2019) 126994.
[2] A. Banerjee, H. Yamamoto, Chem. Sci. 10 (2019) 2124–2129.
[3] X.L. Wu, L.T. Zeng, B.Q. Chen, et al., J. Mater. Chem. B 7 (2019) 5775–5781.
[4] Q.Y. Luo, X.H. Huang, Y. Luo, et al., Chem. Eng. J. 407 (2020) 127050.
[5] Q.J. Liu, L.S. Fan, Q. Zhang, et al., ChemSusChem 10 (2017) 3098–3104.
[6] F. Kastanek, P. Topka, K. Soukup, et al., J. Clean. Prod. 125 (2016) 309–313.
[7] H. Ohtani, K. Takeuchi, Y. Iiguni, et al., Anal. Appl. Pyrolysis 124 (2017) 677–681.
[8] T.R. Lin, M.Q. Zhang, F.H. Xu, et al., Sens. Actuators B: Chem. 261 (2018) 379–384.
[9] A.I. Saiz, G.D. Manrique, R. Fritz, J. Agric. Food Chem. 49 (2001) 98–102.
[10] B.L. Li, S.J. Zhao, L. Huang, et al., Chem. Eng. J. 408 (2020) 127245.
[11] G. Gao, Y.W. Jiang, H.R. Jia, J.J. Yang, F.G. Wu, Carbon 134 (2018) 232–243.
[12] M.H. Lan, S.J. Zhao, S.L. Wu, et al., Nano Res. 12 (2019) 2576–2583.
[13] N.K.R. Bogireddya, J. Larab, L.R. Fragosob, V. Agarwal, Chem. Eng. J. 401 (2020) 126097.
[14] T. Xu, S.J. Zhao, X.L. Wu, L.T. Zeng, M.H. Lan, ACS Sustain. Chem. Eng. 8 (2020) 6413–6421.
[15] X.W. Tian, L. Zhao, Y.X. Pang, D.Y. Li, X.B. Yang, J. Agric. Food Chem. 65 (2017) 9553–9558.
[16] X.C. Li, S.J. Zhao, B.L. Li, et al., Coord. Chem. Rev. 431 (2021) 213686.
[17] Q.H. Zhu, W.L. Yuan, L. Zhang, et al., Anal. Chem. 91 (2019) 6593–6599.
[18] Y.V. Suseela, N. Narayanaswamy, S. Pratihar, T. Govindaraju, Chem. Soc. Rev. 47 (2018) 1098–1131.
[19] T. Li, J.F. Sun, J.Y. Liu, et al., Chin. Chem. Lett. 31 (2020) 439–442.
[20] X.K. Chen, X.D. Zhang, F.G. Wu, Chin. Chem. Lett. 32 (2021) 3048–3052.
[21] S.J. Zhao, S.L. Wu, Q.Y. Jia, et al., Chem. Eng. J. 388 (2020) 124212.
[22] C. Zhang, X.C. Li, T.T. Li, et al., Anal. Chem. 93 (2021) 5145–5150.
[23] M.L. Liu, L. Yang, R.S. Li, et al., Green Chem. 19 (2017) 3611–3617.
[24] X. Geng, Y.Q. Sun, Y.F. Guo, et al., Anal. Chem. 92 (2020) 7940–7946.
[25] M. Li, X.N. Li, M.Y. Jiang, et al., Chem. Eng. J. 399 (2020) 125741.
[26] A.Y. Chen, W.B. Liang, H.J. Wang, et al., Anal. Chem. 92 (2020) 1379–1385.
[27] Y.H. Shi, Y.H. Sun, X.W. Qu, et al., Food Chem. 347 (2021) 129069.
[28] S.Y. Lu, L.Z. Sui, J.J. Liu, et al., Adv. Mater. 29 (2017) 1603443.
[29] X.X. Ye, Y.H. Xiang, Q.R. Wang, Z. Li, Z.H. Liu, Small 15 (2019) 1901673.